energies

MDPI

*Article*

# Investigation of an Innovative Rotor Modification for a Small-Scale Horizontal Axis Wind Turbine

**Artur Bugała * and Olga Roszyk**

Poznan University of Technology, 60–965 Poznań, Poland; olga.roszyk@student.put.poznan.pl

* Correspondence: artur.bugala@put.poznan.pl

Received: 20 April 2020; Accepted: 19 May 2020; Published: 22 May 2020

**Abstract:** This paper presents the results of the computational fluid dynamics (CFD) simulation of the airflow for a 300 W horizontal axis wind turbine, using additional structural elements which modify the original shape of the rotor in the form of multi-shaped bowls which change the airflow distribution. A three-dimensional CAD model of the tested wind turbine was presented, with three variants subjected to simulation: a basic wind turbine without the element that modifies the airflow distribution, a turbine with a plano-convex bowl, and a turbine with a centrally convex bowl, with the hyperbolic disappearance of convexity as the radius of the rotor increases. The momentary value of wind speed, recorded at measuring points located in the plane of wind turbine blades, demonstrated an increase when compared to the base model by 35% for the wind turbine with the plano-convex bowl, for the wind speed of 5 m/s, and 31.3% and 49% for the higher approaching wind speed, for the plano-convex bowl and centrally convex bowl, respectively. The centrally convex bowl seems to be more appropriate for higher approaching wind speeds. An increase in wind turbine efficiency, described by the power coefficient, for solutions with aerodynamic bowls was observed.

**Keywords:** horizontal axis wind turbine; CFD simulation; rotor reshape; renewable energy

## 1. Introduction

Wind energy, next to solar energy and biomass technologies, is becoming ever more important due to its wide availability and low impact on the environment, as its use helps to reduce the emission of gaseous and dust pollutants arising from the combustion of conventional fuels. Considering the axis of rotation, two solutions can be distinguished: HAWT (horizontal axis wind turbine) and VAWT (vertical axis wind turbine). Although HAWT turbines are mainly used on large wind farms, benefits can also be gained through the use of small-scale horizontal axis wind turbines, as in the case of globally developing prosumer installations. It is currently estimated that, in the year 2020, the number of prosumer installations in Poland, using wind turbines and photovoltaic installations, exceeded 160,000, and their total installed power is approaching 1000 MW [1]. Regardless of the scale of the installation, the aerodynamics of the wind flow around the turbine plays an important role in wind turbine efficiency.

An analysis of the literature regarding the various aspects of rotor aerodynamics shows that there are three approaches that can be applied to analyze the airflow around a wind turbine. These are wind tunnel experimental measurements (expensive and highly complex), analytical modeling (limited accuracy), and numerical techniques in the field of fluid mechanics (CFD), which are universal and allow the acceleration of the design and implementation of new solutions, and also verification of errors at an early stage of the project.

Fluid mechanics is the branch of mechanics which touches upon the issues related to the physics of continuous media and the balance and movement of fluids, as well as their impact on the structures that control their flow area.

The complexity of analytical solutions speaks for the legitimacy of the application of new numerical methods in the fluid mechanics branch, in order to obtain an approximate solution.

Many research studies have been conducted with regards to the structure of the airflow through the blades of horizontal axis wind turbines, the design of blade shapes, or the use of various aerodynamic profiles of the blades. Due to the development of computer-aided design codes, a growing number of researchers are using Computational Fluid Dynamics (CFD) to study wind turbine wake aerodynamics.

Reference [2] presents the investigations into the efficiency of wind turbines, using three different CFD methods: an actuator disk, an actuator line, and a fully resolved rotor, using two types of software, i.e., OpenFOAM and ANSYS Fluent. The authors performed simulations of a small-scale wind turbine model, using CFD methods, and obtained a good correlation between the results of measurements and calculations of horizontal wake velocity profiles performed in a wind tunnel, and the results obtained in the Ansys Fluent software, using fully resolved rotor calculations. Furthermore, the authors emphasized that this fact might even contribute to the replacement of the few and expensive wind tunnels.

Many technical and design parameters have an impact on the energy efficiency of a wind turbine. Ngala et al. [3] investigated the performance of a micro horizontal axis wind turbine, using CFD code FLUENT 6.3, including parameters such as the blade chord length, lift force, drag force, tip speed ratio, solidity, angle of attack wind relative angle, Reynolds number, and axial and induction factors. The results were experimentally verified by testing a physically developed wind turbine.

In order to extract the maximum kinetic energy from the wind, researchers put a lot of effort into the design of a blade with effective geometry. In one study [4], the authors used the CFD code to aid them in the blade optimization problem for a small horizontal axis wind turbine, thus obtaining ten-times-greater power in the newly designed blades than that of the original blades. Aerodynamic performance analyses of two different types of horizontal axis wind turbine blades—the classic type (according to the Blade Element Momentum Theory) and the non-twisted type with a constant chord length—were conducted by Meng-Hsien Lee et al. [5]. Wind tunnel experiments to measure the power coefficients of both models, along with numerical simulations to visualize the airflow field for various wind speeds, showed that the maximum power coefficient of the BEMT blade was increased by 50%.

In their study [6], Sudarsono et al. performed a 3D CFD simulation of a modified small-scale NACA 4415 HAWT rotor to determine the rotor's optimum geometry for wind speeds (3, 4, 5, 6, and 7 m/s.). The authors predicted the power output and coefficient by using Blade Element Momentum Theory based on the Lifting Line Theory (LLT). In 2019 Mezaal et al. [7] analyzed the airflow field around the horizontal axis wind turbine with a blade 43.2 m long, conducting static three-dimensional CFD simulations, using the ANSYS Fluent 18.0 software. The test results were validated with theoretical calculations, which agreed with the simulations. Maalawi and Badawy [8] tried to improve the blade performance by obtaining an optimum beam width and turning angle in their study. Xudong et al. [9] tried to design an optimum wind turbine blade, with maximum performance, by taking the beam width, the rotation angle, and the blade thickness into account in their study. In 2015, Abdelrahman et al. [10] used CFD modeling to analyze the impact of different blade shapes with the same radius and airfoil profile (NACA 4418) on turbine performance, including the effect of nacelle, shaft, and tower existence. The authors investigated the following blade shapes: optimal twist and tapered; un-tapered and optimal twist; tapered un-twisted; and un-tapered un-twisted.

A computational fluid dynamics analysis of the HAWT blade cross-section at various blade angles, with the help of ANSYS Fluent, was carried out by Khaled et al. [11]. The authors optimized the chord and twist distributions of the wind turbine blades, to enhance the aerodynamic

performance of the wind turbine, and concluded that the turbine power depends on the blade profile and its orientation.

Many specialized aerofoils have been invented for wind turbine blades, even including different aerofoils in different sections. In one study [12], Chandrala et al. performed an analysis of the HAWT blade (NACA 4420 airfoil) at various blade angles, with the help of ANSYS CFX, and compared their results with experimental research. The authors presented the velocity distribution for various blade angles and stated that, for the tested HAWT, constant power can be obtained between blade angles 22.5° and 60°. Yigit and Durmaz [13] presented the performance of a new blade profile, which was modified from the NACA 0012 profile. In the case of the NACA 0012 profile and the modified profile, an increase between 7.76% and 9.51% in the drag force at low angle of attack was obtained for the modified profile. Moreover, an increase in the lift force, ranging between 9.48% and 10.01%, was obtained. Erisen and Bakirci [14] proposed new profiles derived from the NACA 0012 and NACA 4412 profiles and, using the CFD method, showed that the lift force increases depending on changes in the blade profile based on aerodynamic admittance. In another study [15], the authors designed a blade for a horizontal axis wind turbine with a TSR of 8 and radius 10 m, using the NACA 63–615 airfoil. Computational Fluid Dynamics simulations using the ANSYS Fluent package were used to study the characteristics of the airflow over the designed blade. An analysis regarding the impact of the blade profile type on the wind turbine performance, using CFD calculations, was also presented by Sayed et al. in [16], where the authors used the S809 and S826 blade profiles at different mean wind speeds, for the wind conditions in Egypt.

Another modification which affects the aerodynamic properties of a wind turbine is the use of winglets. In one study [17], the authors performed numerical calculations of the aerodynamics around a wind turbine blade, with and without a winglet, using the ANSYS code. The purpose of the winglet was to decrease the induced drag from the blade. The authors showed that an additional modification of the blade tip leads to increased mechanical power. A similar situation was described in [18], where the authors used the CREO and ANSYS Fluent 14.5 software to obtain the aerodynamic characteristics of small wind turbine rotor blades, with and without an added winglet. The authors concluded that a smaller curvature radius, along with a sufficient height of the winglet, added to the wind turbine rotor, captured more energy in the low wind-speed region when compared to plain wind turbine rotors without the winglet.

The procedure of the accurate design of micro wind turbines, for operation in low airflows, using BEM modeling, CFD calculations and experiments in the aerodynamic tunnel and taking into account the technical issues described above, was presented in [19], where the authors proved that the results of computer simulations and the results of measurements carried out in a subsonic wind tunnel were similar for two wind turbines. The motivation for this research was to emphasize the existence of alternative methods that allow us to increase the efficiency of wind energy conversion into mechanical and electrical energy. It is also important to gain new knowledge on the CFD methods available for wind turbine performance simulations. The simulation tests conducted are an introduction into the laboratory tests currently performed, using specially designed multi-shaped bowls and HAWT-300 wind turbines. The design modifications presented in this paper can contribute to an increase in the appeal of small wind turbines with a horizontal axis of rotation, commonly used in low-power installations also in Poland.

## 2. Materials and Methods

The optimization of mini and micro wind turbines is essential due to the increasing interest in the widespread generation of electrical power [20,21]. Usage of small wind turbines, which are generally designed and optimized for local electrical power generation, are limited due to moderate self-starting conditions, low-wind-speed conditions, and energy efficiency [22].

Due to the fact that a large majority of scientists, in their publications on improving wind turbine design, raise issues related to the optimal blade-shape design [23–27] and appropriate airfoil profile [28,29], alternative research has been proposed, focusing on the aerodynamics of the

introduced multi-shaped bowls, which modify the wind flow in the central part of the wind turbine rotor.

The governing equations for fluid flow are the Navier–Stokes or momentum equation, Equations (2)–(4); the continuity equation, Equation (1); and the energy equation, Equation (5). These equations describe how the velocity, temperature, pressure, and density of a moving fluid are related to each other. With regard to the flow conditions, the Navier–Stokes equations can be rearranged. For low values of the Reynolds number, the inertial effects are assumed to be negligible. The governing partial differential equations, which allow for the description of the movement of a viscous fluid for such structures as wind turbines, can be written as follows [30,31]:

$$\frac{\partial \rho}{\partial t} + \frac{\partial (\rho u)}{\partial x} + \frac{\partial (\rho v)}{\partial y} + \frac{\partial (\rho w)}{\partial z} = 0 \tag{1}$$

$$\frac{\partial (\rho u)}{\partial t} + \frac{\partial (\rho u^2)}{\partial x} + \frac{\partial (\rho uv)}{\partial y} + \frac{\partial (\rho uw)}{\partial z} = -\frac{\partial p}{\partial x} + \frac{1}{\mathrm{Re}}\left[\frac{\partial \tau_{xx}}{\partial x} + \frac{\partial \tau_{xy}}{\partial y} + \frac{\partial \tau_{xz}}{\partial z}\right] \tag{2}$$

$$\frac{\partial (\rho v)}{\partial t} + \frac{\partial (\rho uv)}{\partial x} + \frac{\partial (\rho v^2)}{\partial y} + \frac{\partial (\rho vw)}{\partial z} = -\frac{\partial p}{\partial y} + \frac{1}{\mathrm{Re}}\left[\frac{\partial \tau_{xy}}{\partial x} + \frac{\partial \tau_{yy}}{\partial y} + \frac{\partial \tau_{yz}}{\partial z}\right] \tag{3}$$

$$\frac{\partial (\rho w)}{\partial t} + \frac{\partial (\rho uw)}{\partial x} + \frac{\partial (\rho vw)}{\partial y} + \frac{\partial (\rho w^2)}{\partial z} = -\frac{\partial p}{\partial z} + \frac{1}{\mathrm{Re}}\left[\frac{\partial \tau_{xz}}{\partial x} + \frac{\partial \tau_{yz}}{\partial y} + \frac{\partial \tau_{zz}}{\partial z}\right] \tag{4}$$

$$\begin{aligned}&\frac{\partial (E_T)}{\partial t} + \frac{\partial (uE_T)}{\partial x} + \frac{\partial (vE_T)}{\partial y} + \frac{\partial (wE_T)}{\partial z} = -\frac{\partial (up)}{\partial x} - \frac{\partial (vp)}{\partial y} - \frac{\partial (wp)}{\partial z} - \frac{1}{\mathrm{Re}\,\mathrm{Pr}}\left[\frac{\partial q_x}{\partial x} + \frac{\partial q_y}{\partial y} + \frac{\partial q_z}{\partial z}\right] \\ &+ \frac{1}{\mathrm{Re}}\left[\frac{\partial}{\partial x}(u\tau_{xx} + v\tau_{xy} + w\tau_{xz}) + \frac{\partial}{\partial y}(u\tau_{xy} + v\tau_{yy} + w\tau_{yz}) + \frac{\partial}{\partial z}(u\tau_{xz} + v\tau_{yz} + w\tau_{zz})\right]\end{aligned} \tag{5}$$

where $u$, $v$, and $w$ are the velocity components; $x$, $y$, and $z$ are the coordinates of the spatial domain; $p$ is the pressure; $\tau$ is the components of the stress tensor; $E_T$ is the total energy; $q$ is the heat flux; $Re$ is the Reynolds number, the ratio of the scaling of the inertia of the flow to the viscous forces in the flow; and $Pr$ is the Prandtl number, the ratio of the viscous stresses to the thermal stresses.

The basic test object is the HAWT-300 horizontal axis wind turbine, with a rated power of 300 W, designed to work with an electrochemical energy storage system, using a hybrid charge controller.

Images of the referenced wind turbine and the computer model are presented in Figure 1.

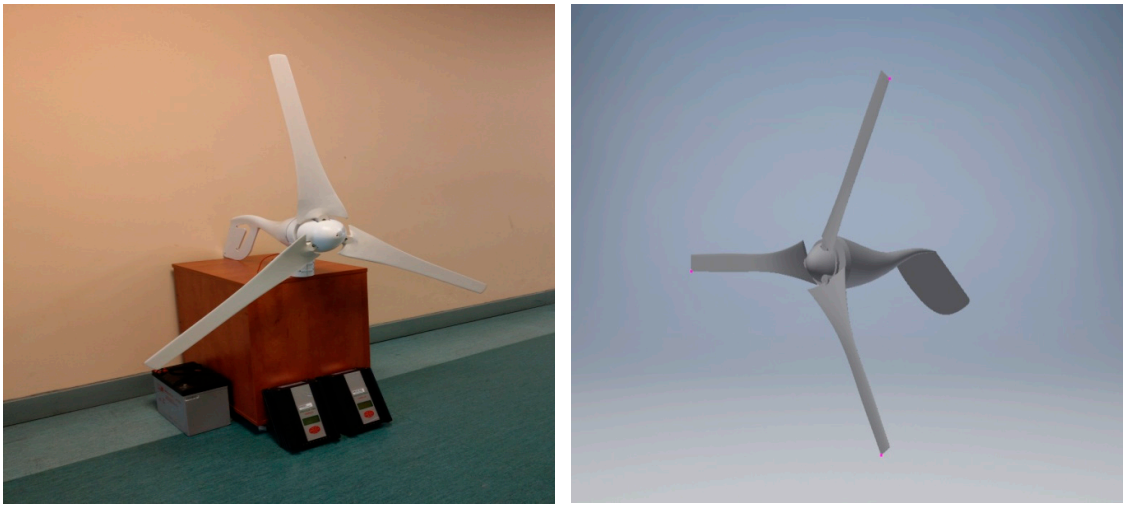

**Figure 1.** HAWT-300 wind turbine and its three-dimensional computer model.

The analyzed wind turbine is characterized by its start, rated, maximum, and survival speeds of 2.5, 11, 20, and 40 m/s, respectively. The twisted blades secured to the aluminum hub were made of carbon fiber, which ensures their rigidity and low weight, along with sufficient durability. The wind turbine is provided with a three-phase AC generator. The turbine deceleration takes place as a result of contact between phase wires. The power characteristics of the analyzed wind turbine are presented in Figure 2.

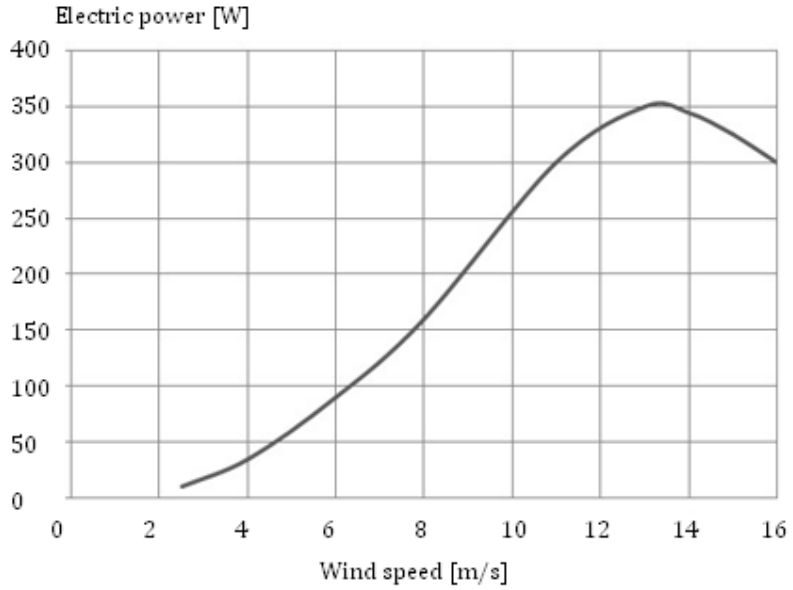


**Figure 2.** Power curve of the tested HAWT-300 wind turbine.

The power coefficient, $C_p$, was determined for the basic wind turbine, as well as a turbine with a plano-convex bowl and a turbine with a centrally convex bowl, based on the following relationship:

$$C_p = 4 \cdot \frac{v_1 - v_{12}}{v_1} \left(1 - \frac{v_1 - v_{12}}{v_1}\right)^2 \quad (6)$$

where $v_1$ is the wind speed before the rotor (m/s), $v_2$ is the wind speed behind the rotor (m/s), and $v_{12}$ is the wind speed in the rotor space

## 3. Computer Simulation Analysis

### *3.1. Simulation Model and Geometry*

In order to carry out the CFD simulation, based on a real wind turbine, a geometrical model was developed by using tools for computer-aided design (CAD) software. The wind turbine presented in Figure 1 was modified with a plano-convex bowl *PW* (Figure 3) and a *CWHZ* bowl which was convex in the center, with a hyperbolic disappearance of convexity at sites distant from the axis of rotation of the rotor (Figure 4).

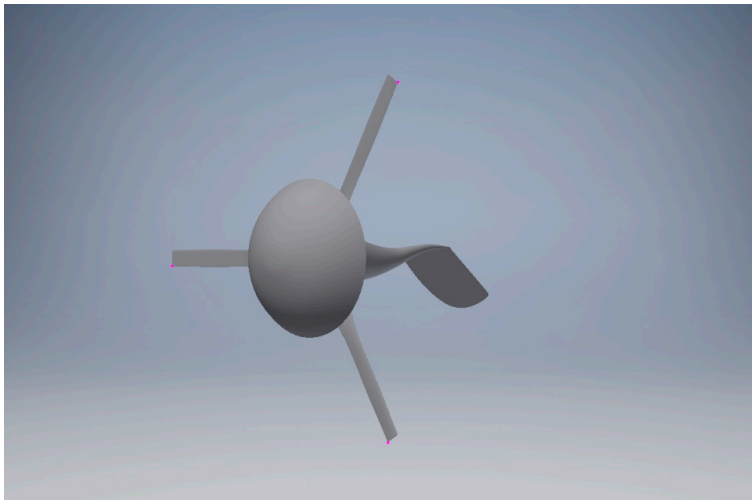

**Figure 3.** HAWT-300 turbine model with an additional plano-convex bowl *PW*.

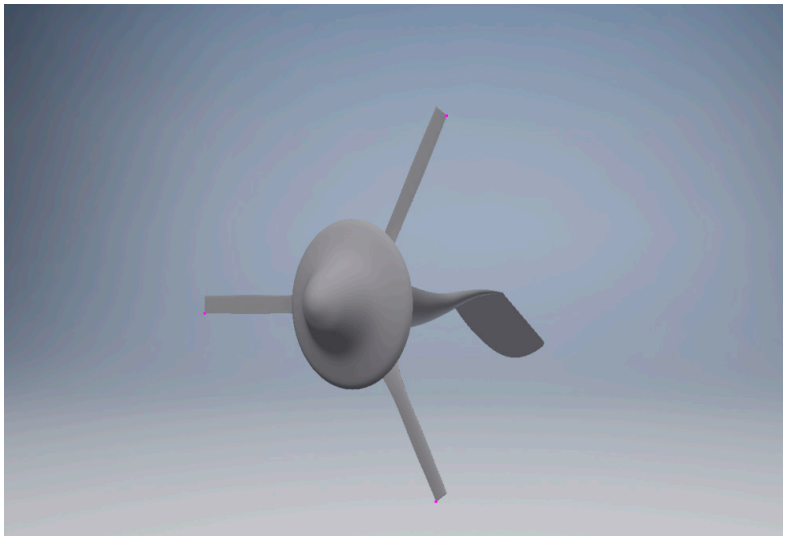

**Figure 4.** HAWT-300 turbine model with an additional centrally convex bowl *CWHZ*.

### *3.2.* Computer Simulation Parameters

In the preprocessor simulation phase, the physical model was converted into a geometric model. The developed models of the wind turbines were enclosed in a cuboid, which is a representation of a three-dimensional space for the airflow. The cuboidal control volume was divided into many smaller elements, forming the numerical grid. The mesh grid is concentrated close to the blade, where the flow changes are more intense, in the calculation domain, because of the computational accuracy. In the simulation, an unstructured tetrahedral mesh was used to discretize the models. Unstructured grids allow the solution of a large detailed problem in a relatively short period of time. The mesh was selected to obtain compaction of the elements in places with higher velocity gradients, especially near the edges of the turbine blades, to better capture the boundary layer. In the far-field, the mesh resolution can become progressively coarser. The generated mesh (Figure 5) shows the high density of the elements on the tip of the blades and around the leading edge. To check how the numerical mesh behaves with different sizes of the control volume, in particular in the area of the blades, different meshes were also generated.

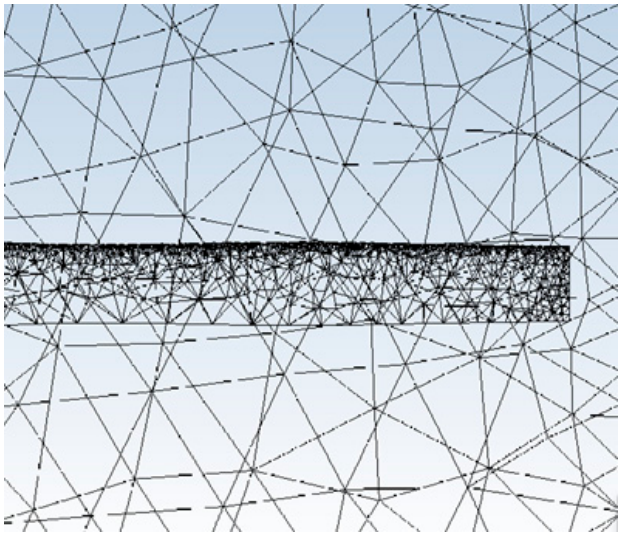

**Figure 5.** The form of the numerical mesh used in the simulation, including areas in close distance to the edges of the blade.

A numerical mesh of test objects was created. To increase the accuracy of the calculations, the mesh should be large enough to avoid boundary effects. For the wind turbine model with the plano-convex bowl *PW* and centrally convex bowl *CWHZ*, the number of mesh elements exceeds 340,000.

Fluid was defined as incompressible and laminar. Boundary conditions were set. Two types of boundary conditions were used, namely velocity inlet (5, 10, 15, 20, and 25 m/s) and pressure outlet. The density of the air was $\rho = 1.20473$ kg.m$^{-3}$, and the dynamic viscosity was $\mu = 1.817 \times 10^{-5}$ kg/m.s. The values of the operating pressure and temperature were set at the levels of 101325 Pa and 293 K, respectively. An image of the whole geometric model is presented in Figure 6.

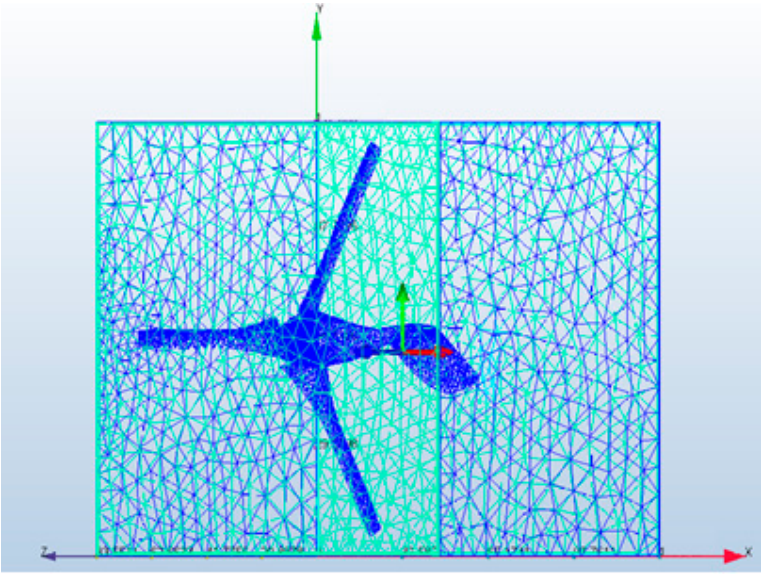

**Figure 6.** Numerical mesh generated for the tested wind turbine model—HAWT-300.

A Segregated Solver was utilized in the CFD calculations. In order to solve approximations to the flow equations in the analyzed problem, the Finite Element Method was used. In the Segregated Solver the governing equations can be solved separately. The x-momentum, y-momentum, and z-momentum equations can be solved, respectively, for U at all of the nodes, for V at all of the nodes, and for W at all of the nodes, whereby each U, V, and W are associated with the pressure parameter

by the relationship deduced from the momentum equations. Since a single degree of freedom is solved at a time, less memory resources are required. A simplified sequence of the operations in the solver used is presented in Figure 7.

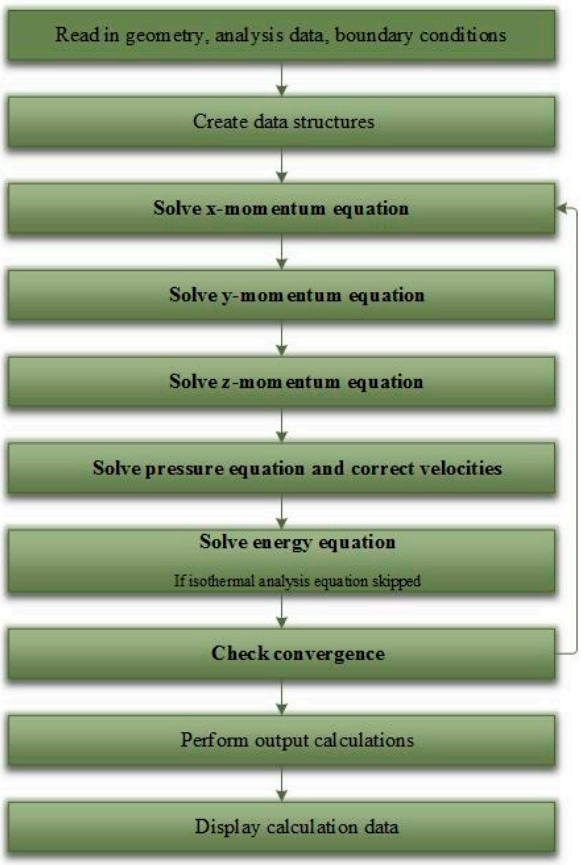


**Figure 7.** Sequence of operations in the CFD simulation performed by using the Segregated Solver.

The governing equations, describing the flow problem for the analyzed wind turbines, are solved iteratively. With each iteration, the calculated estimates come closer to the correct solution. The total number of selected iterations is 35. The performed CFD simulation can also be stopped after checking and reaching the convergence criterion. The measure of convergence in the calculations is the residual norm.

Discretization of governing equations, using the Finite Element Method, leads to their transition to algebraic equations for dependent variables. After this process, an equation for each finite element node in the analysis model is obtained for each dependent variable. The algebraic equations are solved to determine the values of the dependent variables in nodes. The nodal residual of the equation at node *i* is defined as follows:

$$R_{\phi,i} = F_i - A_{ii}\phi_i - \sum_{j \neq i} A_{ij}\phi j \quad (7)$$

where $A_{ij}$ represents algebraic coefficients resulting from discretizing, and $F_i$ represents the discretized source terms.

After the global iteration, the norm of the nodal residuals is calculated as the square root of the algebraic sum of all nodal residual squares and decreases as the result of calculations approximates the expected correct result.

## 4. Results of the CFD Simulation

The postprocessor simulation stage includes an analysis of the solution results. A quantitative evaluation of the analyzed models of wind turbines, with and without the modifying element, was performed on the basis of the designated wind-speed distributions on consecutive parallel planes, located on the axis from the three-dimensional coordinate system. Plane number 1 is the plane determined by the rotating blades of the wind turbine. The measuring points were located on the surface of the respective blades. The view of the analyzed spatial plane of the measuring solid in the Autodesk Simulation CFD is presented in Figure 8.

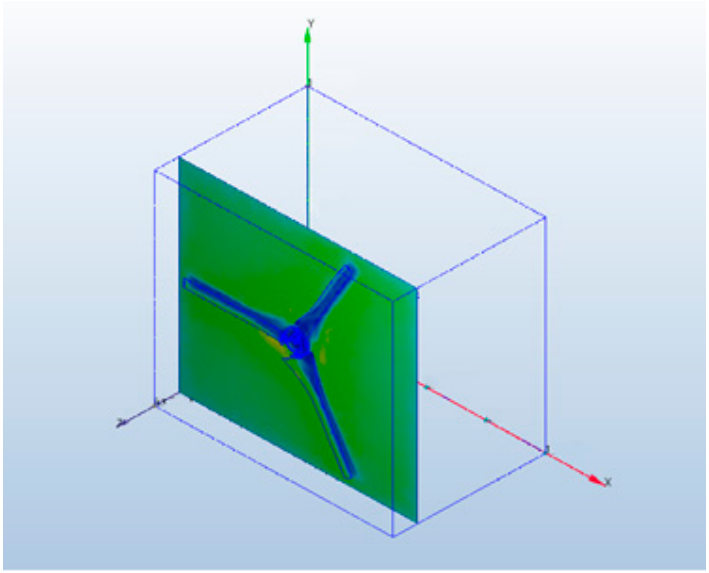

**Figure 8.** View of the selected measuring plane of momentary wind-speed values for the HAWT-300 wind turbine model.

The location of the measuring points on the blade surfaces for the three analyzed wind turbine models and the results of the computer simulation for the distribution of wind approaching with a speed of 20 m/s is presented in Figures 9–11.

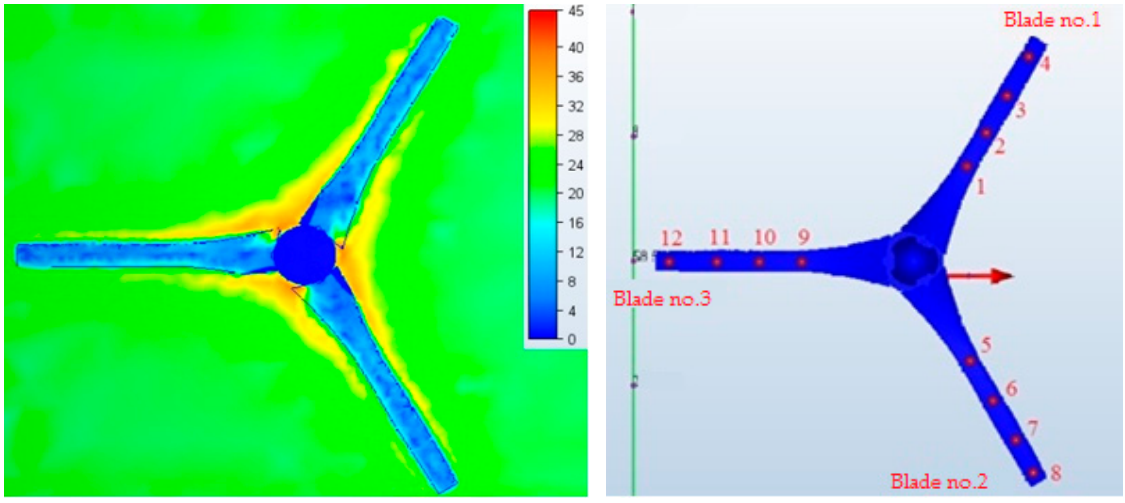

**Figure 9.** Location of the measuring points and distribution of wind speeds for the HAWT-300 turbine model without the modifying element.

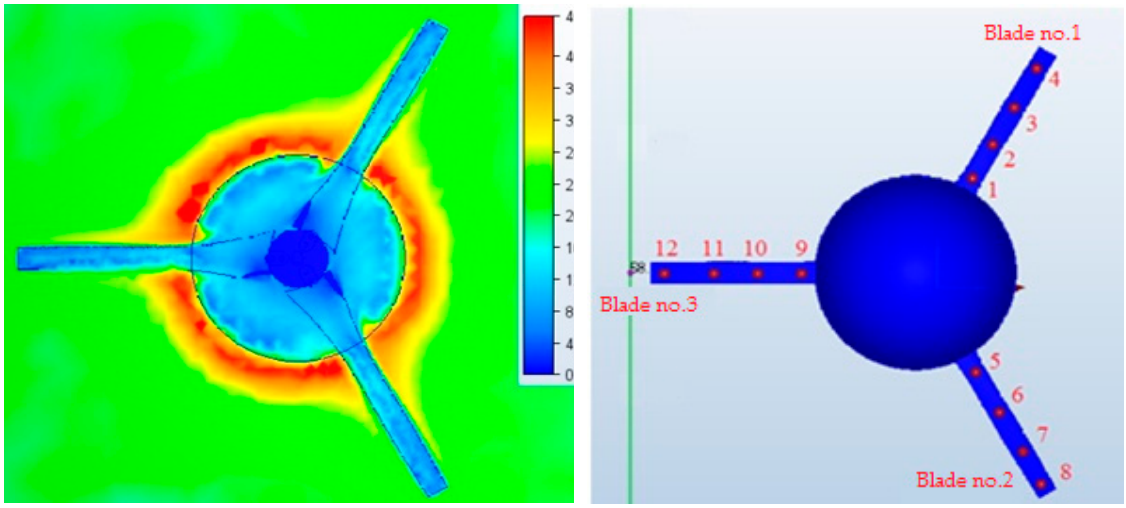


**Figure 10.** Location of the measuring points and distribution of wind speeds for the HAWT-300 turbine model with the plano-convex bowl PW.

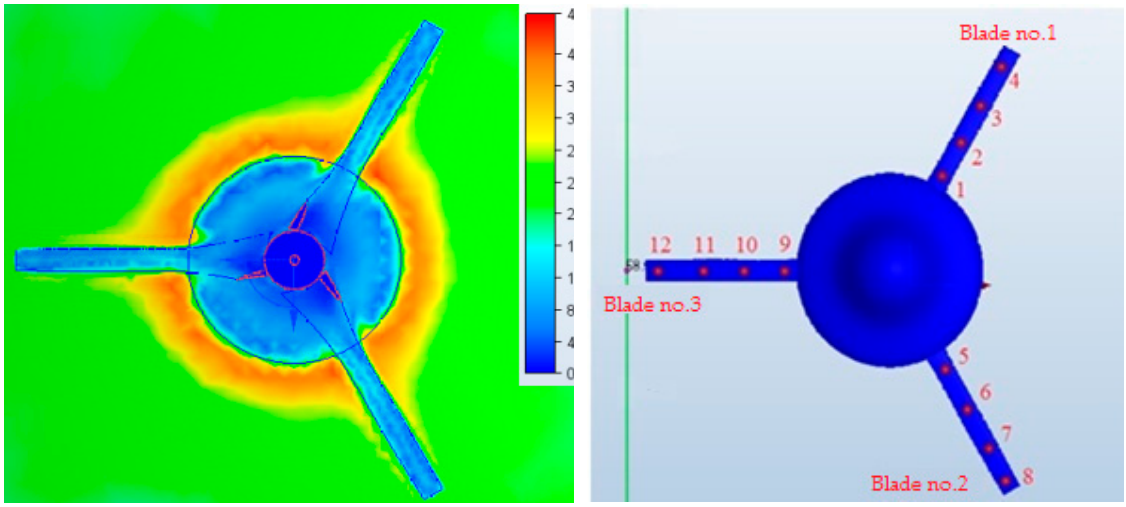


**Figure 11.** Location of the measuring points and distribution of winds speeds for the HAWT-300 turbine model with the centrally convex bowl *CWHZ*.

The full results of the simulation calculations for the wind-speed values at measuring points for each of the three models, using the Autodesk Simulation CFD software, are presented in Tables 1–5.

**Table 1.** Results of calculations for the set wind speed of 5 m/s.

| Set Wind Speed $v_z$ (m/s) | Blade No. | Point No. | Base Model | | PW Model | | CWHZ Model | |
|---|---|---|---|---|---|---|---|---|
| | | | Wind Speed at the Point v (m/s) | $v/v_z$ (%) | Wind Speed at the Point v (m/s) | $v/v_z$ (%) | Wind Speed at the Point v (m/s) | $v/v_z$ (%) |
| 5 | 1 | 1 | 1.45 | 29.00 | 2.13 | 42.60 | 2.15 | 43.00 |
| | | 2 | 1.60 | 32.00 | 1.98 | 39.60 | 1.53 | 30.60 |
| | | 3 | 1.42 | 28.40 | 1.70 | 34.00 | 1.28 | 25.60 |
| | | 4 | 1.66 | 33.20 | 2.00 | 40.00 | 1.11 | 22.20 |
| | | **Average** | 1.53 | 30.65 | 1.95 | 39.05 | 1.52 | 30.35 |
| | | **σ** | 0.10 | - | 0.16 | - | 0.39 | - |
| | 2 | 5 | 1.64 | 32.80 | 2.49 | 49.80 | 2.25 | 45.00 |
| | | 6 | 1.36 | 27.20 | 2.15 | 43.00 | 1.55 | 31.00 |
| | | 7 | 1.50 | 30.00 | 1.66 | 33.20 | 0.95 | 19.00 |
| | | 8 | 1.62 | 32.40 | 2.09 | 41.80 | 1.29 | 25.80 |
| | | **Average** | 1.53 | 30.60 | 2.10 | 41.95 | 1.51 | 30.20 |
| | | **σ** | 0.11 | - | 0.30 | - | 0.48 | - |
| | 3 | 9 | 1.69 | 33.80 | 2.61 | 52.20 | 2.34 | 46.80 |
| | | 10 | 1.57 | 31.40 | 2.32 | 46.40 | 1.80 | 36.00 |
| | | 11 | 1.70 | 34.00 | 1.94 | 38.80 | 1.27 | 25.40 |
| | | 12 | 1.30 | 26.00 | 1.88 | 37.60 | 1.14 | 22.80 |
| | | **Average** | 1.57 | 31.30 | 2.17 | 43.75 | 1.64 | 30.75 |
| | | **σ** | 0.16 | - | 0.30 | - | 0.47 | - |

**Table 2.** Results of calculations for the set wind speed of 10 m/s.

| Set Wind Speed $v_z$ (m/s) | Blade No. | Point No. | Base Model | | PW Model | | CWHZ Model | |
|---|---|---|---|---|---|---|---|---|
| | | | Wind Speed at the Point v (m/s) | $v/v_z$ (%) | Wind Speed at the Point v (m/s) | $v/v_z$ (%) | Wind Speed at the Point v (m/s) | $v/v_z$ (%) |
| 10 | 1 | 1 | 2.60 | 26.00 | 5.13 | 51.30 | 6.57 | 65.70 |
| | | 2 | 2.82 | 28.20 | 6.59 | 65.90 | 5.99 | 59.90 |
| | | 3 | 2.71 | 27.10 | 4.36 | 43.60 | 4.87 | 48.70 |
| | | 4 | 3.45 | 34.50 | 4.11 | 41.10 | 5.14 | 51.40 |
| | | **Average** | 2.90 | 28.95 | 5.05 | 50.48 | 5.64 | 56.63 |
| | | **σ** | 0.33 | - | 0.97 | - | 0.71 | - |
| | 2 | 5 | 2.66 | 26.60 | 4.89 | 48.90 | 6.67 | 66.70 |
| | | 6 | 2.59 | 25.90 | 6.68 | 66.80 | 5.34 | 53.40 |
| | | 7 | 3.01 | 30.10 | 3.89 | 38.90 | 5.25 | 52.50 |
| | | 8 | 3.42 | 34.20 | 3.66 | 36.60 | 5.39 | 53.90 |
| | | **Average** | 2.92 | 29.20 | 4.78 | 47.80 | 5.66 | 56.43 |
| | | **σ** | 0.33 | - | 1.19 | - | 0.58 | - |
| | 3 | 9 | 3.08 | 30.80 | 5.33 | 53.30 | 7.65 | 76.50 |
| | | 10 | 3.28 | 32.80 | 6.13 | 61.30 | 5.96 | 59.60 |
| | | 11 | 3.21 | 32.10 | 5.02 | 50.20 | 4.36 | 43.60 |
| | | 12 | 2.73 | 27.30 | 3.89 | 38.90 | 5.04 | 50.40 |
| | | **Average** | 3.08 | 30.75 | 5.09 | 50.93 | 5.75 | 57.53 |
| | | **σ** | 0.21 | - | 0.80 | - | 1.23 | - |

**Table 3.** Results of calculations for the set wind speed of 15 m/s.

| Set Wind Speed $v_z$ (m/s) | Blade No. | Point No. | Base Model | | PW Model | | CWHZ Model | |
|---|---|---|---|---|---|---|---|---|
| | | | Wind Speed at the Point v (m/s) | $v/v_z$ (%) | Wind Speed at the Point v (m/s) | $v/v_z$ (%) | Wind Speed at the Point v (m/s) | $v/v_z$ (%) |
| 15 | 1 | 1 | 7.03 | 46.87 | 8.31 | 55.40 | 10.08 | 67.20 |
| | | 2 | 4.60 | 30.67 | 8.30 | 55.33 | 8.04 | 53.60 |
| | | 3 | 4.49 | 29.93 | 5.84 | 38.93 | 7.18 | 47.87 |
| | | 4 | 7.68 | 51.20 | 7.21 | 48.07 | 7.26 | 48.40 |
| | | **Average** | 5.95 | 39.67 | 7.42 | 49.43 | 8.14 | 54.27 |
| | | **σ** | 1.42 | - | 1.01 | - | 1.17 | - |
| | 2 | 5 | 6.66 | 44.40 | 6.69 | 44.60 | 9.85 | 65.67 |
| | | 6 | 4.35 | 29.00 | 7.78 | 51.87 | 7.31 | 48.73 |
| | | 7 | 5.80 | 38.67 | 7.10 | 47.33 | 7.46 | 49.73 |
| | | 8 | 4.86 | 32.40 | 6.06 | 40.40 | 8.02 | 53.47 |
| | | **Average** | 5.42 | 39.12 | 6.91 | 46.05 | 8.16 | 54.4 |
| | | **σ** | 0.89 | - | 0.63 | - | 1.01 | - |
| | 3 | 9 | 4.84 | 32.27 | 8.63 | 57.53 | 10.87 | 72.47 |
| | | 10 | 6.38 | 42.53 | 7.51 | 50.07 | 8.04 | 53.60 |
| | | 11 | 4.32 | 28.80 | 6.55 | 43.67 | 5.79 | 38.60 |
| | | 12 | 4.30 | 28.67 | 5.64 | 37.60 | 7.53 | 50.20 |
| | | **Average** | 4.96 | 33.07 | 7.08 | 47.22 | 8.06 | 53.72 |
| | | **σ** | 0.85 | - | 1.11 | - | 1.83 | - |

**Table 4.** Results of calculations for the set wind speed of 20 m/s.

| Set Wind Speed $v_z$ (m/s) | Blade No. | Point No. | Base Model | | PW Model | | CWHZ Model | |
|---|---|---|---|---|---|---|---|---|
| | | | Wind Speed at the Point v (m/s) | $v/v_z$ (%) | Wind Speed at the Point v (m/s) | $v/v_z$ (%) | Wind Speed at the Point v (m/s) | $v/v_z$ (%) |
| 20 | 1 | 1 | 9.17 | 45.85 | 10.90 | 54.50 | 13.46 | 67.30 |
| | | 2 | 4.99 | 24.95 | 10.44 | 52.20 | 10.88 | 54.40 |
| | | 3 | 5.96 | 29.80 | 8.51 | 42.55 | 9.83 | 49.15 |
| | | 4 | 9.08 | 45.40 | 10.29 | 51.45 | 9.66 | 48.30 |
| | | **Average** | 7.30 | 36.50 | 10.04 | 50.18 | 10.96 | 54.79 |
| | | **σ** | 1.86 | - | 0.91 | - | 1.52 | - |
| | 2 | 5 | 8.65 | 43.25 | 10.91 | 54.55 | 13.00 | 65.00 |
| | | 6 | 5.40 | 27.00 | 9.77 | 48.85 | 9.94 | 49.70 |
| | | 7 | 7.30 | 36.50 | 9.38 | 46.90 | 10.64 | 53.20 |
| | | 8 | 5.61 | 28.05 | 8.78 | 43.90 | 10.37 | 51.85 |
| | | **Average** | 6.74 | 33.70 | 9.71 | 48.55 | 10.99 | 54.94 |
| | | **σ** | 1.33 | - | 0.78 | - | 1.19 | - |
| | 3 | 9 | 6.51 | 32.55 | 12.72 | 63.60 | 14.58 | 72.90 |
| | | 10 | 7.92 | 39.60 | 9.50 | 47.50 | 11.10 | 55.50 |
| | | 11 | 4.96 | 24.80 | 7.71 | 38.55 | 7.56 | 37.80 |
| | | 12 | 4.58 | 22.90 | 8.75 | 43.75 | 10.07 | 50.35 |
| | | **Average** | 5.99 | 29.96 | 9.67 | 48.35 | 10.83 | 54.14 |
| | | **σ** | 1.33 | - | 1.87 | - | 2.52 | - |

**Table 5.** Results of calculations for the set wind speed of 25 m/s.

| Set Wind Speed $v_z$ (m/s) | Blade No. | Point No. | Base Model | | PW Model | | CWHZ Model | |
|---|---|---|---|---|---|---|---|---|
| | | | Wind Speed at the Point v (m/s) | $v/v_z$ (%) | Wind Speed at the Point v (m/s) | $v/v_z$ (%) | Wind Speed at the Point v (m/s) | $v/v_z$ (%) |
| 25 | 1 | 1 | 8.13 | 32.52 | 8.96 | 35.84 | 16.58 | 66.32 |
| | | 2 | 4.88 | 19.52 | 8.73 | 34.92 | 13.39 | 53.56 |
| | | 3 | 5.34 | 21.36 | 7.29 | 29.16 | 12.38 | 49.52 |
| | | 4 | 8.89 | 35.56 | 10.08 | 40.32 | 11.39 | 45.56 |
| | | **Average** | 6.81 | 27.24 | 8.77 | 35.06 | 13.44 | 53.74 |
| | | **σ** | 1.73 | - | 3.94 | - | 1.95 | - |
| | 2 | 5 | 7.44 | 29.76 | 9.33 | 37.32 | 15.95 | 63.80 |
| | | 6 | 5.64 | 22.56 | 8.30 | 33.20 | 12.79 | 51.16 |
| | | 7 | 6.73 | 26.92 | 8.38 | 33.52 | 13.24 | 52.96 |
| | | 8 | 6.75 | 27.00 | 8.75 | 35.00 | 12.32 | 49.28 |
| | | **Average** | 6.64 | 26.56 | 8.69 | 34.76 | 13.58 | 54.30 |
| | | **σ** | 0.64 | - | 0.41 | - | 1.41 | - |
| | 3 | 9 | 6.63 | 26.52 | 9.89 | 39.56 | 17.48 | 69.92 |
| | | 10 | 7.49 | 29.96 | 7.57 | 30.28 | 13.41 | 53.64 |
| | | 11 | 5.55 | 22.20 | 6.91 | 27.64 | 8.66 | 34.64 |
| | | 12 | 5.52 | 22.08 | 8.35 | 33.40 | 12.17 | 48.68 |
| | | **Average** | 6.30 | 25.19 | 8.18 | 32.72 | 12.93 | 51.72 |
| | | **σ** | 0.82 | - | 1.11 | - | 3.15 | - |

Figures 12–16 show the average wind-speed values determined from the measuring points for each blade, taking into account the base model of the wind turbine, as well as *PW* model and *CWHZ* model.

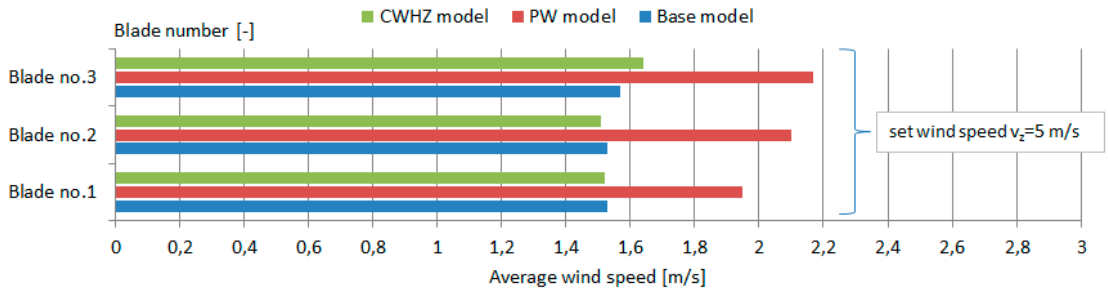


**Figure 12.** Average wind-speed values calculated from the measuring points located on each blade, including the base, *PW*, and *CWHZ* wind turbine model, for the set wind speed of 5 m/s.

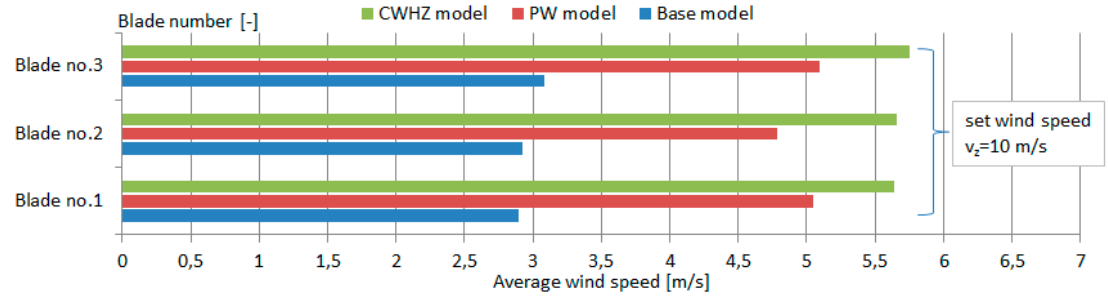

**Figure 13.** Average wind-speed values calculated from the measuring points located on each blade, including the base, *PW*, and *CWHZ* wind turbine model, for the set wind speed of 10 m/s.

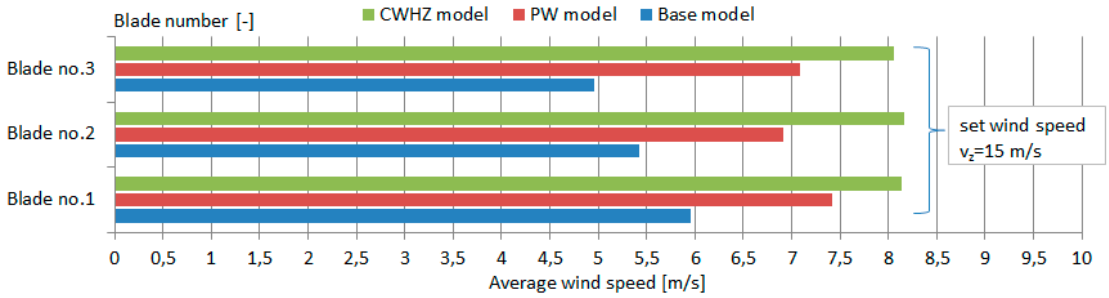


**Figure 14.** Average wind-speed values calculated from the measuring points located on each blade, including the base, *PW*, and *CWHZ* wind turbine model, for the set wind speed of 15 m/s.

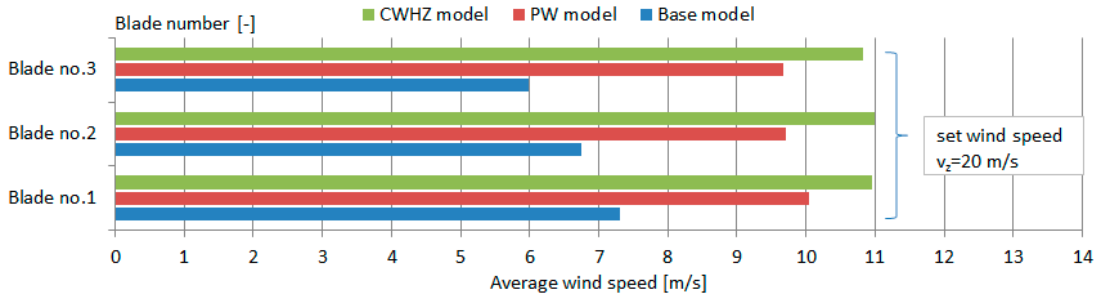


**Figure 15.** Average wind-speed values calculated from the measuring points located on each blade, including the base, *PW*, and *CWHZ* wind turbine model, for the set wind speed of 20 m/s.

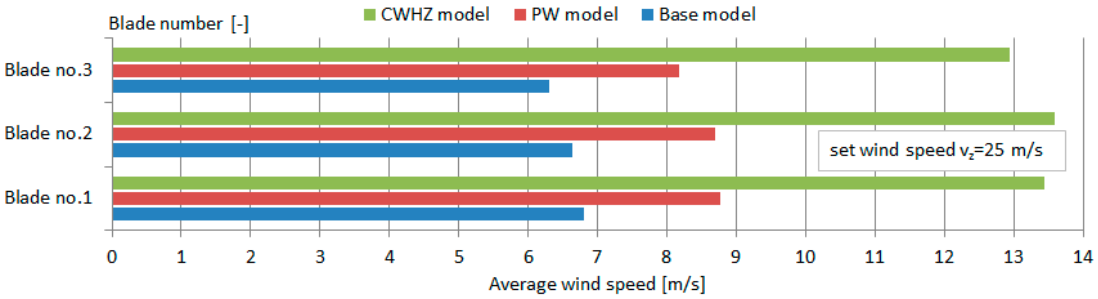


**Figure 16.** Average wind-speed values calculated from the measuring points located on each blade, including the base, *PW*, and *CWHZ* wind turbine model, for the set wind speed of 25 m/s.

A comparison of power output and power coefficient for a wind turbine with a plano-convex bowl and centrally convex bowl in relation to basic model is presented in Figures 17 and 18.

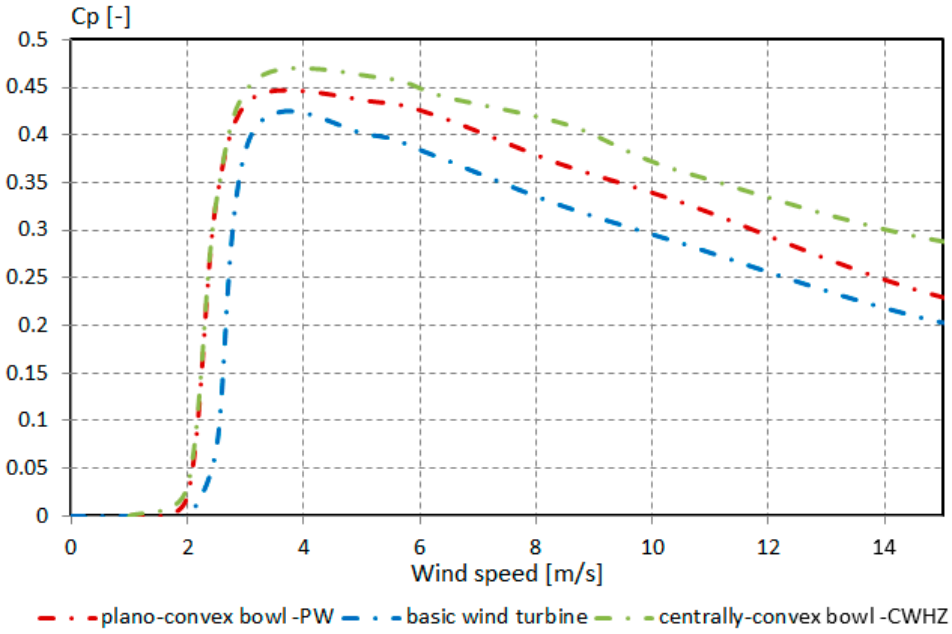


**Figure 17.** Power coefficient variation as a function of a wind speed for analyzed wind turbines.

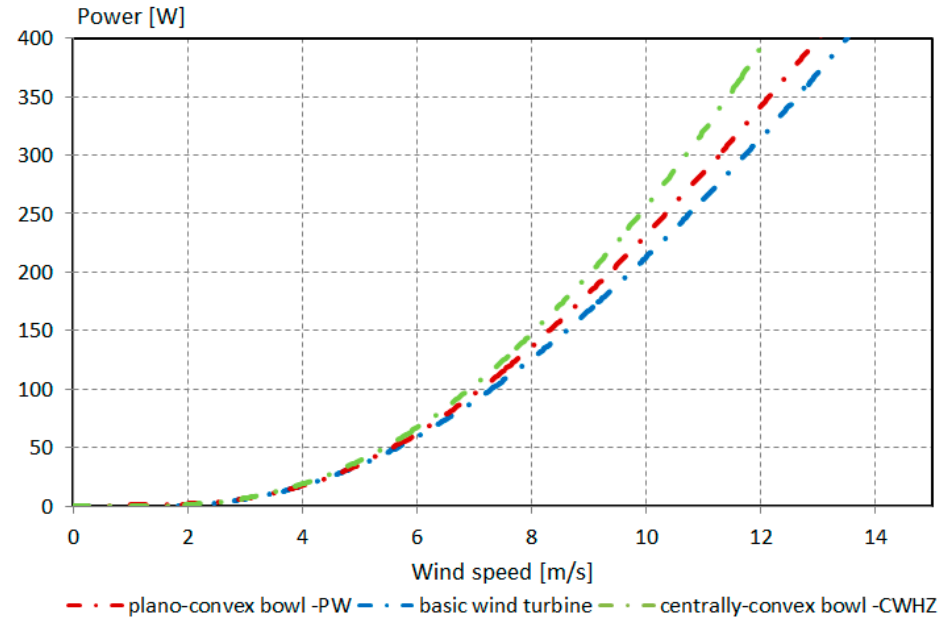


**Figure 18.** Power variation as a function of a wind speed for analyzed wind turbines.

## 5. Discussion

The purpose of the conducted simulation tests was to determine the legitimacy of using additional structural elements which modify the rotor space and are adapted to the structure of the tested wind turbine. The tested elements complement the classic structure of the horizontal axis wind turbine, and their implementation does not require any additional structural changes in the further structures of the wind turbine.

While analyzing the distribution of wind-speed values at different measuring points on wind turbine blades, it is possible to notice that the highest wind-speed values are still registered in the center of the structure, in the axis of rotation of the rotor (Figures 9–11). This fact justifies further research aimed at designing and testing wind turbine rotor bowls of other shapes and sizes.

However, it should be emphasized that the results obtained for the analyzed wind turbines with plano-convex and centrally convex bowls indicate a better use of the incoming wind than in the case of the basic wind turbine.

In the case of the wind turbine model with the plano-convex bowl *PW* (Figure 3), a significant increase in the wind speed is observed on the perimeter of the bowl (Figure 10). A part of the airflow moves behind the wind turbine. A change in the shape of the bowl to *CWHZ* leads to a reduction in this effect. The shape of the bowl directs the air stream toward the rotor plane, which is also noticeable at the ends of the blades, where in the case of the wind turbine with the *PW* bowl, lower speeds of the wind reaching the areas more distant from the axis of rotation of the rotor are observed.

While comparing the obtained simulation results, it must be concluded that, in almost every analyzed case, the use of additional bowls increases the speed of the wind blowing at a given measuring point located on the blade of a wind turbine. In the case of the base wind turbine, without the modifying element, the change in the wind-speed value ranging between 5 and 25 m/s, with 5 m/s increments, results in the obtainment of an average wind speed, calculated on the basis of 12 measuring points, i.e., 1.54, 2.96, 5.44, 6.68, and 6.58 m/s, respectively. This gives 30.8%, 29.6%, 36.3%, 33.4%, and 26.3% of the excitation speed value.

The use of the wind turbine with the plano-convex bowl *PW* allows for an increase in the average value of wind speed, calculated on the basis of 12 measuring points, by 35% for the wind speed of 5 m/s, when compared to the unmodified turbine. An increase in the value of the speed of the approaching wind to 15 m/s leads to 31.3% and 49% increases in the average wind speed as a result of the use of the *PW* and *CWHZ* bowls (Figure 14). An increase in the wind speed above 5 m/s and the use of the *CWHZ* bowl allow for the observation of 57%, 54%, 55%, and 53% of the excitation speed value of the wind (10, 15, 20, and 25 m/s), respectively. Changing the shape of the modifying element to the plano-convex one leads to the observation of 49%, 48%, 49%, and 34% excitation speed value. It seems that the plano-convex bowl *PW* is more appropriate for lower approaching wind speeds (Figure 12). The use of the *CWHZ* bowl for the low wind-speed values limits the potential benefits resulting from the use of additional structural elements in the rotor space.

By determining the ratio of the difference between the average wind-speed value from measuring points located on the plane of the blades, using the plano-convex bowl and the turbine model without the bowl, and the excitation speed of the wind, it must be concluded that the use of the *CWHZ* bowl for higher approaching wind speeds is more effective in comparison to the use of the *PW* bowl (Figures 13–16). For the set speed of 10 m/s, the value of the calculated parameter for the model of the wind turbine with the CWHZ bowl is approximately 7%; for 15 m/s, it is approximately 6.5%; for 20 m/s, it is 5.6%; and for 25 m/s, it is approximately 17.6%.

The simulation for the set speed equal to 25 m/s was performed outside the operating range of the wind turbine. A decrease in the average value of wind speed, determined by measurements performed at 12 measuring points, is noticeable in relation to the trend for the speeds ranging between 5 and 20 m/s for the reference turbine and the model of the turbine with the convex bowl.

The use of a centrally convex bowl (*CWHZ*) and plano-convex bowl (*PW*) leads to an increase in the maximum value of the $C_p$ coefficient by 14.9% and 9.9% in relation to the value obtained for the basic wind turbine (Figure 17). In the range of higher wind speeds, the use of the centrally convex bowl allows higher power coefficient value to be longer maintained. A higher value of the $C_p$ parameter affects the value of obtained power (Figure 18). The convergence of the obtained power results is particularly noticeable in the range of low wind-speed values. By increasing the wind-speed value in the range of 6–8 m/s, it is possible to obtain a percentage increase in the generated instantaneous power—in relation to the basic wind turbine—by 38% and 14%, using a centrally convex bowl and a plano-convex bowl, respectively. The energy benefit of using aerodynamic bowls increases as the wind speed reaches the rated speed for the wind turbine.

A higher uniformity of distribution is observed for the lower-excitation wind-speed values measured at the measuring points located on wind turbine blades, and this is confirmed by the lower value of the determined standard deviation, $\sigma$ (Tables 1–5).

## 6. Conclusions

The displacement of the airflow from the central part of the rotor, which is a place with a limited energy potential, may enable the generation of a higher mechanical power from the kinetic energy of the approaching wind, whose value depends, to a great extent, on the wind-speed value. The addition bowls, attached to the center of the turbine rotor, redirect the wind that would have otherwise passed through the blades. The application of force at a greater distance from the axis of the rotor hub may result in movement of the rotor at a lower initial speed of the approaching wind. Wind is less effective when it flows into a fragment of the blade near the rotor hub.

By adding a fluid-redirecting device to an existing wind turbine, it is also possible to better adapt the small wind turbine to local wind conditions. As shown in this work, it is possible to design bowls with shapes more suitable for low wind-speed values and shapes for higher values.

It should be emphasized that the mesh quality and domain size of the CFD models, accurate wind turbine CAD models, careful consideration of the measurement data, the computational setup, and flow input parameters affect the quality and stability of the analysis and convergence time.

Testing of HAWT-300 wind turbines, currently conducted on the premises of the Poznan University of Technology, including the designed and physically available elements of different shapes which modify the rotor space under real operating conditions, are valuable complements of the presented simulation work. The tested wind turbines, which work with a hybrid charge controller, accumulate energy in electrochemical energy storages in the form of gel batteries, demonstrating initially higher values of such parameters as electrical voltage on generator terminals and charge current, as a consequence of incorporation of the tested bowls.

The use of additional tested elements modifying the airflow distribution in the form of aerodynamic bowls may be justified. The efficiency of the wind turbine, however, depends on its shape, geometrical dimensions, and type of material. The effect of use of the bowls also depends on the speed of the approaching wind.

This research is of a developmental nature. Other airflow conditions are being tested, and calculations for turbulent flows are being performed, as well. Other shapes of bowls are also being designed.

**Author Contributions:** Design analysis of wind turbine models was developed by O.R.; the simulation tests presented in this manuscript and their evaluation were carried out by A.B. and O.R.; A.B. supervised the research and prepared the manuscript. All authors have read and agreed to the published version of the manuscript.

**Funding:** This research received no external funding.

**Conflicts of Interest:** The authors declare no conflict of interest.

## Nomenclature

| Acronym | Meaning | Units |
|---|---|---|
| AC | Alternating Current | - |
| BEMT | Blade Element Momentum Theory | - |
| CAD | Computer Aided Design | - |
| CFD | Computational Fluid Dynamics | - |
| $C_P$ | Power Coefficient | - |
| CWHZ | Bowl convex in the center, with a hyperbolic disappearance of convexity at sites distant from the axis of rotation of the rotor | - |
| FEM | Finite Element Method | - |
| HAWT | Horizontal Axis Wind Turbine | - |
| LLT | Lifting Line Theory | - |
| $\mu$ | Dynamic viscosity | kg/m.s. |
| p | Pressure | Pa |
| Pr | Prandtl number | - |
| PW | Bowl plano-convex | - |
| $\sigma$ | Standard deviation | - |

| | | |
|---|---|---|
| Re | Reynolds number | - |
| $R_{\varphi,i}$ | Nodal residual at node *i* | - |
| ϱ | Density of the air | $kg.m^{-3}$ |
| TSR | Tip Speed Ratio | - |
| τ | Components of the stress tensor | - |
| u | Velocity component in x direction | $m.s^{-1}$ |
| v | Velocity component in y direction | $m.s^{-1}$ |
| VAWT | Vertical Axis Wind Turbine | - |
| w | Velocity component in z direction | $m.s^{-1}$ |

## References


1. URE. Available online: www.ure.gov.pl (accessed on 4 February 2020).
2. Kalvig, S.; Manger, E.; Hjertager, B. Comparing different CFD wind turbine modelling approaches with wind tunnel measurements. In Proceedings of the The Science of Making Torque from Wind, Oldenburg, Germany, 9–11 October 2012.
3. Okeola, F.O.; Odebunmi, E.O.; Ameen, O.M.; Amoloye, M.A.; Lawal, A.A.; Abdulmumeen, A.G. *Arid Zone J. Eng. Technol. Environ.* **2015**, *11*, 13–23.
4. Cheng, C.Y.; Song, D.H.; Tsai, G.C. CFD Analysis and Blade Optimization of a Small Horizontal Axis Wind Turbine. *Adv. Mat. Res.* **2012**, *591*, 231–235.
5. Lee, M.H.; Shiah, Y.C.; Bai, C.J. Experiments and numerical simulations of the rotor-blade performance for a small-scale horizontal axis wind turbine. *J. Wind Eng. Ind. Aerodyn*. **2016**, *149*, 17–29.
6. Sudarsono, S.; Susastriawan, A.; Sugianto, S. Three-dimensional CFD Analysis of Performance of Small-scale Hawt based on Modified NACA-4415 Airfoil. *Int. J. Technol.* **2019**, *10*, 212.
7. Mezaal, N.A.; Osintsev, K.V.; Alyukov, S.V. The computational fluid dynamics performance analysis of horizontal axis wind turbine. *Int. J. Power Electron. Drive Syst.* **2019**, *10*, 1072–1080.
8. Maalawi, K.Y.; Badawy, M.T.S. A direct method for evaluating performance of horizontal axis wind turbines. *Renew. Sustain. Energy Rev.* **2001**, *5*, 175–190, doi:10.1016/S1364-0321(00)00017-4.
9. Xudong, W.; Shen, W.Z.; Zhu, W.J.; Sørensen, J.N.; Jin, C. Shape optimization of wind turbine blades. *Wind Energy* **2009**, *12*, 781–803, doi:10.1002/we.335.
10. Abdelrahman, M.A.; Abdellatif, O.E.; Moawed, M.; Eliwa, A.; Mišák, S. The CFD performance analysis for horizontal axis wind turbine with different blade shapes and tower effect. In Proceedings of the 16th International Scientific Conference on Electric Power Engineering (EPE), Kouty nad Desnou, Czech, 20–22 May 2015; pp. 754–759.
11. Khaled, M.; Ibrahim, M.M.; Hamed, H.E.A.; Gawad, A.F.A. Aerodynamic Design and Blade Angle Analysis of a Small Horizontal–Axis Wind Turbine. *Am. J. Mod. Energy* **2017**, *3*, 23–37.
12. Chandrala, M.; Choubey, A.; Gupta, B. Aerodynamic Analysis of Horizontal Axis Wind Turbine Blade. *Int. J. Eng. Res. Appl.* **2012**, *3*, 1244–1248.
13. Yigit, C.; Durmaz, U. Wind Turbine Blade Design with Computational Fluid Dynamics Analysis. *Int. J. Comput. Exp. Sci. Eng.* **2017**, *3*, 44–49.
14. Duquette, M.M.; Visser, K.D. Numerical Implications of Solidity and Blade Number on Rotor Performance of Horizontal-Axis Wind Turbines. *J. Sol. Energy Eng.* **2003**, *125*, doi:10.1115/1.1629751.
15. Younas, M.F.; Ali, A.; Shafique, M.D. CFD Simulation of HAWT Blade and Implementation of BEM Theory. *Sukkur IBA J. Emerg. Technol.* **2019**, *2*, 21–35.
16. Sayed, M.A.; Kandil, H.A.; Morgan, E.I. Dynamic stall analysis of horizontal-axis-wind-turbine blades using computational fluid dynamics. *AIP Conf. Proc.* **2012**, *1440*, 953.
17. Congedo, P.M.; De Giorgi, M.G. Optimizing of a wind turbine rotor by CFD modeling. In Proceedings of the 2008 ANSYS Italian Conference: Inspiring Engineering and Sciences, Venice, Italy, 16–17 October 2008.
18. Premalatha, P.; Rajakumar, S. Design of the small horizontal axis wind turbine blade with and without winglet. *Int. J. Res. Sci. Technol.* **2016**, *6*, 2249-0604.
19. Lanzafame, R.; Messina, M.M. Numerical and experimental analysis of micro HAWTs designed for wind tunnel applications. *Int. J. Energy Environ. Eng.* **2016**, *7*, 199–210.
20. Foster, E.; Contestabile, M.; Blazquez, J.; Manzano, B.; Workman, M.; Shah, N. The unstudied barriers to widespread renewable energy deployment: Fossil fuel price responses. *Energy Policy* **2017**, *103*, 258–264, doi:10.1016/j.enpol.2016.12.050.

21. Browne, O.; Poletti, S.; Young, D. How does market power affect the impact of large scale wind investment in 'energy only' wholesale electricity markets? *Energ Policy* **2015**, *87*, 17–27, doi:10.1016/j.enpol.2015.08.030.
22. Wang, F.; Bai, L.; Fletcher, J.; Whiteford, J.; Cullen, D. The methodology for aerodynamic study on a small domestic wind turbine with scoop. *J. Wind Eng. Ind. Aerodyn.* **2008**, *96*, 1–24, doi:10.1016/j.jweia.2007.03.004.
23. Queau, J.P.; Trompette, P. Optimal Shape Design of Turbine Blades. *J. Vib. Acoust. Stress Reliab.* **1983**, *105*, 444–448, doi:10.1115/1.3269126.
24. Anim-Mensah, S. *The Optimum Design of a Wind Turbine Blade: In-depth View*; Lap Lambert Academic Publishing: Germany 2011.
25. Brondsted, P.; Nijssen, R.P.L. *Advances in Wind Turbine Blade Design and Materials*, 1 ed.; Woodhead Publishing: England 2013.
26. Jureczko, K.; Pawlak, M.; Mężyk, A. Optimisation of wind turbine blades. *J. Mater. Process. Technol.* **2005**, *167*, 463–471, doi:10.1016/j.jmatprotec.2005.06.055.
27. Jeong, J.; Park, K.; Junand, S.; Lee, D.H. Design optimization of a wind turbine blade to reduce the fluctuating unsteady aerodynamic load in turbulent wind. *J. Mech. Sci. Technol.* **2012**, *26*, 827–838.
28. Canale, T.; Ismail, K.A.R.; Lino, F.A.M.; Arabkoohsar, A. Comparative Study of New Airfoils for Small Horizontal Axis Wind Turbines. *J. Sol. Energy Eng.* **2020**, *142*, doi:10.1115/1.4046089.
29. Duz, H.; Yildiz, S. Numerical Performance Analyses of Different Airfoils for Use in Wind Turbines. *Int. J. Renew. Energy Dev.* **2018**, *7*, 151–157, doi:10.14710/ijred.7.2.151-157.
30. NASA. Available online: www.grc.nasa.gov (accessed on 1 April 2020).
31. Sanderse, B.; Van der Pijl, S.P.; Koren, B. Review of CFD for wind-turbine wake aerodynamics. *Phys. Rev. Lett.* **2010**, *1*, 1-28.